ORNL/SPR-2023/2948

Machine Learning for Processing Ultrasonic Data from Long-Term Monitoring of Concrete with Alkali-Silica Reaction (ASR)

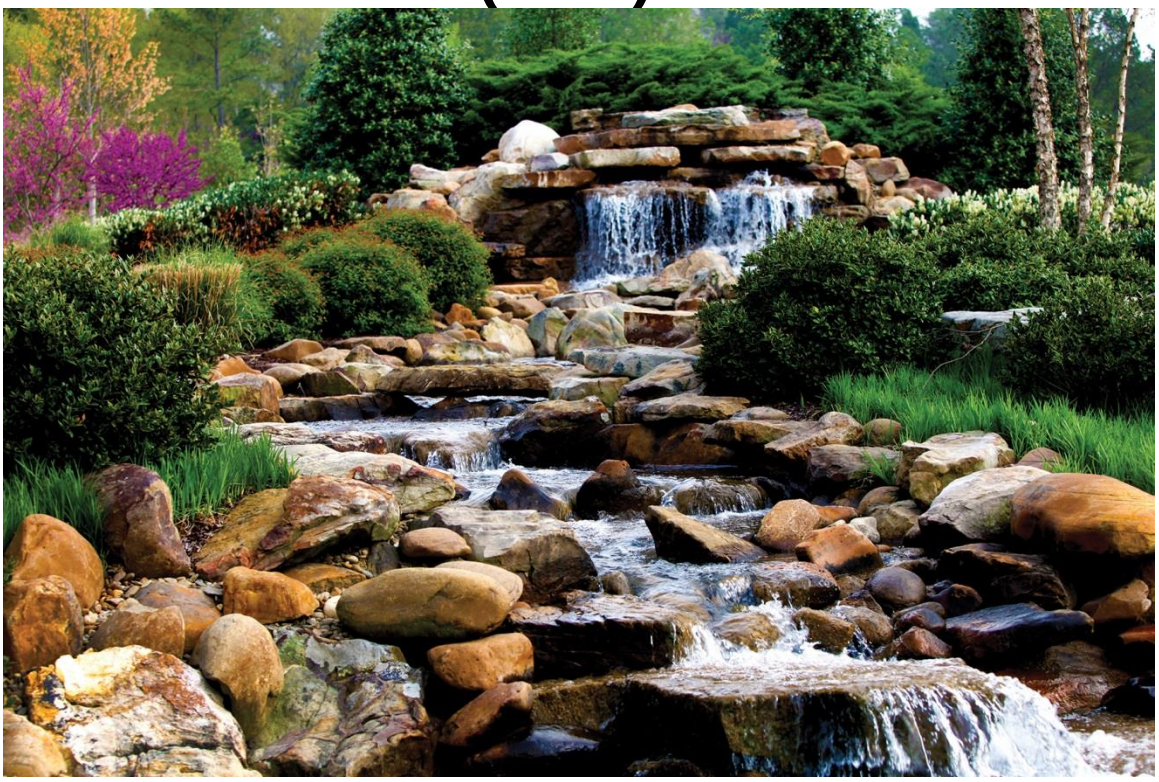

Hongbin Sun
Samantha Sabatino
June 2023

OAK RIDGE National Laboratory

LWRS LIGHT WATER REACTOR SUSTAINABILITY

ORNL IS MANAGED BY UT-BATTELLE LLC FOR THE US DEPARTMENT OF ENERGY

DOCUMENT AVAILABILITY

Reports produced after January 1, 1996, are generally available free via OSTI.GOV.

Website www.osti.gov

Reports produced before January 1, 1996, may be purchased by members of the public from the following source:

National Technical Information Service
5285 Port Royal Road
Springfield, VA 22161
Telephone 703-605-6000 (1-800-553-6847)
TDD 703-487-4639
Fax 703-605-6900
E-mail info@ntis.gov
Website http://classic.ntis.gov/

Reports are available to US Department of Energy (DOE) employees, DOE contractors, Energy Technology Data Exchange representatives, and International Nuclear Information System representatives from the following source:

Office of Scientific and Technical Information
PO Box 62
Oak Ridge, TN 37831
Telephone 865-576-8401
Fax 865-576-5728
E-mail reports@osti.gov
Website https://www.osti.gov/

ORNL/SPR-2023/2948

Light Water Reactor Sustainability Program

M3LW-23OR0403025

Nuclear Energy and Fuel Cycle Division

MACHINE LEARNING FOR PROCESSING ULTRASONIC DATA FROM LONG-TERM MONITORING OF CONCRETE WITH ALKALI-SILICA REACTION (ASR)

Hongbin Sun
Samantha Sabatino

June 2023

Prepared by
OAK RIDGE NATIONAL LABORATORY
Oak Ridge, TN 37831
managed by
UT-BATTELLE LLC
for the
US DEPARTMENT OF ENERGY
under contract DE-AC05-00OR22725

CONTENTS

LIST OF FIGURES

EXECUTIVE SUMMARY

The alkali–silica reaction (ASR) is a phenomenon that leads to material degradation in concrete, resulting in the formation of microcracks and cracks. This deterioration causes a loss of mechanical properties, concrete damage, and even corrosion. To address this issue, ultrasonic nondestructive evaluation can be employed as a technique for long-term monitoring of ASR development and condition assessment of concrete subjected to ASR. However, traditional approaches typically utilize only a few wave parameters, such as wave velocity or amplitude, to characterize ASR-induced concrete damage while disregarding the majority of information present in the ultrasonic signals.

In this study, four machine learning (ML) models were established and comparatively evaluated to establish a relationship between concrete expansion due to ASR and ultrasonic signals. Two concrete specimens intentionally designed to exhibit ASR development were cast and conditioned in a curing chamber to accelerate ASR. Over a span of more than 500 days, ultrasonic signals and expansion data were collected continuously on these specimens. From the ultrasonic signals, wave velocity and 12 wavelet features were extracted and utilized as inputs for three ML models: linear regression, support vector regression, and shallow neural network. Training these models involves employing data from one ASR specimen while testing was performed using data from the other ASR specimen for expansion prediction. In the case of the deep neural network model, preprocessed time domain ultrasonic signals were utilized as inputs without the need for feature engineering. All models underwent optimization based on the training data.

The results demonstrated that the linear regression, support vector regression, and shallow neural network models exhibited poor performance on the test data, yielding prediction R^2 values smaller than 0.71 and root mean square error (RMSE) values larger than 0.09%. Consequently, a feature selection process was implemented, leading to the identification of six features that displayed the highest correlation coefficients with the expansion. By employing these selected six features, all three models exhibited improved performance, with higher R^2 values and smaller RMSE values. Notably, the choice of ML model did not yield significant differences in the results, indicating that the selected features exerted a greater influence on prediction accuracy than the specific ML algorithm used. Furthermore, the deep neural network model produced comparable prediction results to the three models with feature selection, suggesting that deep learning models possess the potential to achieve accurate predictions based on ultrasonic signals without the need for feature engineering.

ACKNOWLEDGMENTS

This research was sponsored by the US Department of Energy (DOE) Office of Nuclear Energy's Light Water Reactor Sustainability program under contract DE-AC05-00OR22725 with UT Battelle LLC/Oak Ridge National Laboratory (ORNL).

1. INTRODUCTION

The alkali–silica reaction (ASR) is a type of material degradation commonly observed in concrete infrastructure. It occurs when reactive vitreous or poorly crystalline silica—such as chert or microcrystalline quartz—present in the aggregate reacts with alkalis in the cement. This reaction generates hydrated sodic or potassium-bearing calcium-silicates gels, known as ASR gel [1]. The ASR gel absorbs water and expands within the material's porosity and existing cracks, creating internal pressure and causing expansion. Eventually, this leads to the formation and propagation of additional cracks in the concrete. Consequently, ASR results in concrete deterioration, loss of mechanical properties, and increased diffusion of aggressive substances. Ultimately, this can lead to corrosion of steel reinforcement and can detrimentally affect the structure's service life.

Currently, ASR condition assessment programs primarily rely on visual inspection. Although concrete coring with subsequent petrographic examination [2] is a reliable method for assessing the presence of ASR, visual inspection remains subjective and does not provide accurate information about internal concrete damage. Moreover, because of the petrographic examination process, the condition assessment procedure involving concrete coring is time-consuming, labor-intensive, and destructive. To address these limitations, nondestructive evaluation (NDE) methods, such as ultrasonic testing, offer a promising solution for evaluating ASR damage in concrete. Various ultrasonic wave parameters, including wave velocity, attenuation, and amplitude, have been used to quantify ASR damage [3]–[5]. As ASR develops, the amplitude and velocity of ultrasonic waves propagating through the concrete decrease, whereas the wave attenuation increases [6].

Since the advent of AI, machine learning techniques (ML) have been frequently employed for the automated analysis of ultrasonic data to characterize the condition and remaining service life of concrete structural elements. Previous works have mainly focused on using ML algorithms to predict concrete strength based on single wave parameters, such as ultrasonic pulse velocity (UPV) and signal amplitude [7]–[10]. However, these approaches utilize only wave velocity information, neglecting other valuable information embedded in the ultrasonic signals, particularly in the frequency domain. Indeed, valuable lessons can be learned from studying the ultrasonic NDE approaches used for the automatic detection of welding defects; these NDE techniques use a variety of features extracted from ultrasonic signals, such as wave parameters, statistical features, and wavelet features [11]–[13]. Thus, similar NDE methodologies can be adopted to extract features from ultrasonic signals in concrete with ASR damage, considering that the ultrasonic signal in damaged concrete is more complex than that in welding defects. Recent studies have also applied ML in the ultrasonic NDE of concrete with ASR damage [14]–[16].

In this study, several ML models were investigated for predicting ASR expansion using long-term monitoring ultrasonic signals obtained from two concrete samples subjected to ASR. The expansion level serves as a measure of the extent of ASR damage in real-world applications. Wave parameters and wavelet features are extracted from the ultrasonic signals and used as input for the ML models. The data from one of the concrete specimens were utilized as the training dataset because this specimen exhibits a large final expansion during the long-term experiment. The data from the second specimen were used as the testing dataset. Feature selection was employed to examine the impact of features on the performance of machine learning models. A deep learning model was also investigated using the time domain signal as the input without requiring explicit feature engineering or user input.

2. CONCRETE SAMPLES AND ULTRASONIC DATA COLLECTION

Two concrete samples (i.e., "ASR" and "ASR-2D"), as shown in Figure 1, were cast with the same 0.3 × 0.3 × 1.12 m dimensions. The ASR and ASR-2D samples used the same mix design, which contains a reactive coarse aggregate. Along with the reactive coarse aggregate, NaOH was added to boost the alkali content to 1.50% Na_2O_{eq} by mass of cement, which promotes rapid ASR in the concrete samples; the mix design is shown in Table 1. Whereas no reinforcing steel bars were added to the ASR sample to allow free expansion, #6 headed steel rebar was installed in the ASR-2D sample in the longitudinal (Y-direction) and vertical (Z-direction) directions to confine the expansion in these directions. More details about the concrete samples can be found in the study by Malone [17], [18]. After 28 days, the samples were moved to a conditioning chamber, where they were kept at 38°C and 90% humidity for more than 500 days to accelerate the ASR development. Demountable mechanical strain gauge (DEMEC) targets were installed on each surface, and the expansions in the three directions were measured using DEMEC strain gauges (Mayes Instruments Limited, United Kingdom) every two weeks when the chamber was temporarily shut down. The volumetric expansion is the summation of the expansions in the three directions. Figure 2 shows the volumetric expansion histories of the ASR and ASR-2D samples for the experiment duration (i.e., 552 days). Numerous surface cracks developed on the ASR and ASR-2D samples, which indicate the success of the ASR promotion in the samples.

Table 1. Mix design of the ASR samples.

Component	Quantity
Cement (kg/m^3)	350
Water (kg/m^3)	175
Coarse aggregate (kg/m^3)	1039
Fine aggregate (kg/m^3)	839
Water reducer (mL/kg)	2.3
50/50 NaOH (kg/m^3)	9.31

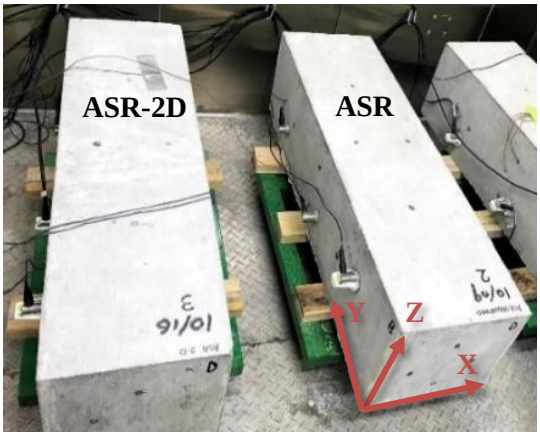

Figure 1. ASR and ASR-2D concrete samples with reactive coarse aggregates.

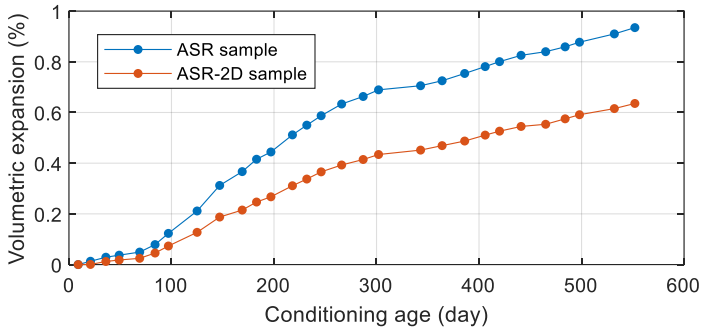

Figure 2. Volumetric expansions for the ASR and ASR-2D samples.

A pair of ultrasonic transducers was installed on the concrete sample permanently for long-term monitoring (see Figure 3). A 15 mm diameter piezoceramic disc (STEMINC) was used as the transmitter, and an acoustic emission (AE) sensor (R15I-AST, Physical Acoustic, New Jersey) with a center frequency of 150 kHz was used as the ultrasonic receiver. A multiplexer was used to switch between different transmitter and receiver pairs. The received signals were digitized by an oscilloscope (PICO4262) with a sampling rate of 10 MHz and averaged by 100 times to increase the signal-to-noise ratio. The ultrasonic signal was collected every 12 hours, along with temperature measurements. Data were not collected during the conditioning chamber shutdowns. More details about the ultrasonic monitoring system can be found in other work by Sun [19]. Overall, 644 ultrasonic signals were collected from the ASR sample, and 620 signals were collected from the ASR-2D sample. Since more ultrasonic signals were recorded than expansion measurements (29 data points), the expansion corresponding to each ultrasonic signal was calculated using linear interpolation. This linear interpolation is justified because the conditioning environment was consistent between two expansion measurements.

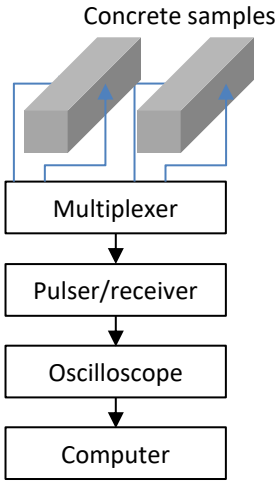

Figure 3. Diagram of the ultrasonic monitoring system for the concrete samples.

3. ULTRASONIC DATA PROCESSING AND FEATURE EXTRACTION

Figure 4 shows the time domain signals at the concrete age of 60, 260, and 460 days for the ASR sample. The first signal (Figure 4(a)) was collected at an early age when the concrete sample exhibited a relatively small expansion; at this time, the ASR may not have initiated, and the signal still contains high-frequency components. In the signal collected at 60 days, the peak amplitude occurs at approximately 0.1 μs. The second signal (Figure 4(b)) was collected at 260 days, and the concrete sample exhibited relatively large expansion due to ASR. The peak amplitude occurs around 0.25 μs, and fewer high-frequency components are observed in the signal, as compared to Figure 4(a). Additionally, the signal amplitude is much lower than the first signal since more energy is attenuated by the concrete cracks resulting from the ASR induced expansion. The third signal (Figure 4(c)) was collected at the late stage of the ASR development with large concrete expansion. The signal also shows a low-amplitude and few high-frequency components. These time domain signals indicate that the ultrasonic signal contains useful information that is related to the status of the ASR development, which is measured by the volumetric expansion.

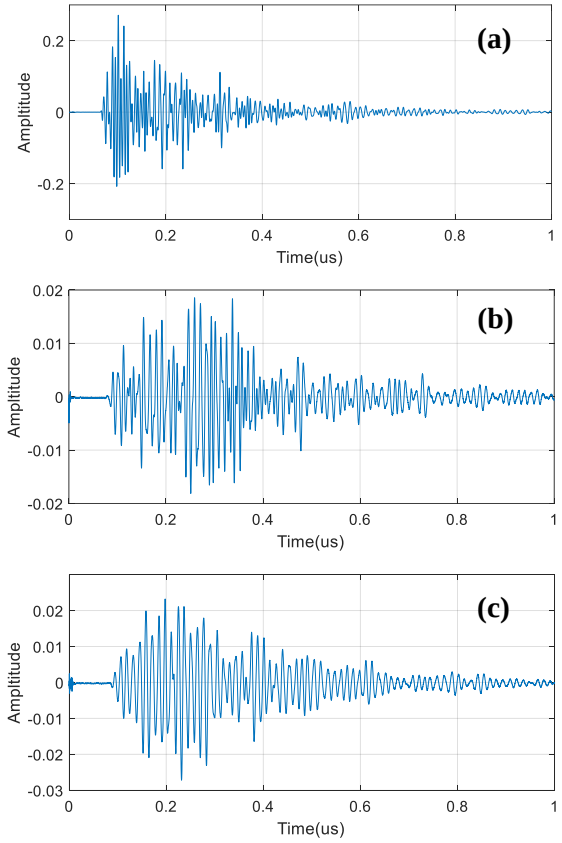

Figure 4. Time domain signals at different concrete ages: (a) 60, (b) 260, and (c) 460 days.

In this work, several features were extracted from the time domain signals for ML model training and testing. These features, along with the expansion data from the ASR sample, are used for model training, and the data collected from the ASR-2D sample will be used for testing the ML models. The data from the ASR and ASR-2D samples are used for training and testing, respectively, because the ASR sample exhibits larger expansion than the ASR-2D sample, thus ensuring that model testing on the ASR-2D sample requires only interpolation and no extrapolation. Two types of features are extracted from the time domain signal. The first is wave velocity, which is directly related to the crack density and concrete modulus. The second parameter extracted includes the wavelet features calculated via discrete wavelet transform, which

decomposes the time domain signal into signals in different frequency bands. After the decomposition, wavelet features are calculated for each band signal.

3.1 ULTRASONIC WAVE VELOCITY

Wave velocity is the most commonly used parameter in ultrasonic nondestructive testing for material characterization. As the ASR sample exhibits gradual cracking, the wave propagation velocity is reduced. In this work, wave velocity is extracted as one of the features used for damage assessment. The Akaike information criterion (AIC) picker was used to detect the arrival time automatically. The AIC picker method was originally developed for analyzing the P-wave velocity of seismic waves [20]. The AIC values are calculated for the first 1,000 points of the time domain signal, and the point with the lowest AIC value represents the first arrival time, which is shown in Figure 5. According to the AIC value curve, the first arrival time is 64.3 μs, when the AIC curve has the smallest value. The wave velocity for the ASR and ASR-2D samples are shown in Figure 6. Both the ASR and ASR-2D samples exhibit a decreasing velocity during the monitoring period. The spikes on the curves are due to the AIC calculation error where the signal is noisy.

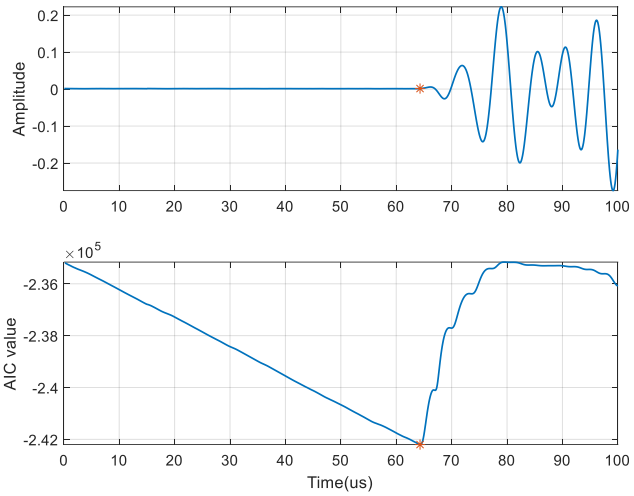

Figure 5. First arrival time in the time domain signal (top) and the AIC values calculated (bottom).

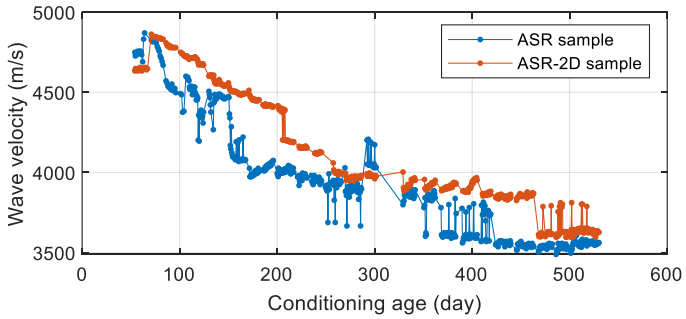

Figure 6. Wave velocity histories for the ASR and ASR-2D samples.

3.2 Wavelet features

Aside from the wave velocity, other features can be extracted from the ultrasonic signals in both the time and frequency domains. Wavelet transform is the technique that processes a signal in the time and frequency domains and has been widely used to extract features from ultrasonic signals in the NDT of welding defects

[11], [21]. Discrete wavelets transform (DWT) is an algorithm that can be used to quickly obtain the wavelet transform coefficients of a discrete time signal. The algorithm decomposes the ultrasonic signal with a low-pass and high-pass filter into its coarse approximation coefficient cA_1 and detail coefficient cD_1. The bandwidth is [0, f/2] for the approximation coefficient cA_1 and [f/2, f] for the detail coefficient cD_1, and f is half of the sampling rate. This process is repeated until the desired decomposition level is achieved. The wavelet feature extraction is based on these detail coefficients.

The ultrasonic signal at the conditioning age of 54 days in Figure 7(a) was decomposed into seven levels with the MATLAB function *modwt* and "db4" wavelet. Before implementing the DWT, each signal is normalized by its amplitude. Because the energy of the original ultrasonic signal is in the frequency range of 40 to 250 kHz (Figure 7(b)), only the last three levels of the detail coefficients were used for the feature extraction. Figures 7(c)–(e) show the detail coefficients cD_5, cD_6, and cD_7 from DWT. Coefficients cD_5 and cD_6 have a higher amplitude than cD_7, which indicates that the original ultrasonic signal has more energy in the high-frequency range (>78 kHz) than at the early conditioning age. For each of the three detail coefficients, four features were extracted. First was the mean amplitude, $A_m = \frac{1}{n}\sum_{i=1}^{n}|x_i|$, where x_i represents the amplitude of each sample in the signal, and n is the total number of samples. As the ASR damage accumulates, the energy decreases in the high-frequency bandwidth and increases in the low-frequency bandwidth. Therefore, the mean value of the detail coefficient will have the same trend as the energy in different bandwidths. The second feature is the maximum amplitude, A_{max}. Similar to the mean amplitude, the maximum amplitude also has the same trend as the energy in different bandwidths. The third feature is the total energy, $E = \sum x_i^2$. The energy ratio in the low-frequency bandwidth increases as the ASR develops. The fourth feature is the attenuation coefficient, which is calculated from the three coefficients by fitting the signal after the maximum amplitude using an exponential decay function. Thirteen features were extracted from each ultrasonic signal: twelve wavelet features and wave velocity.

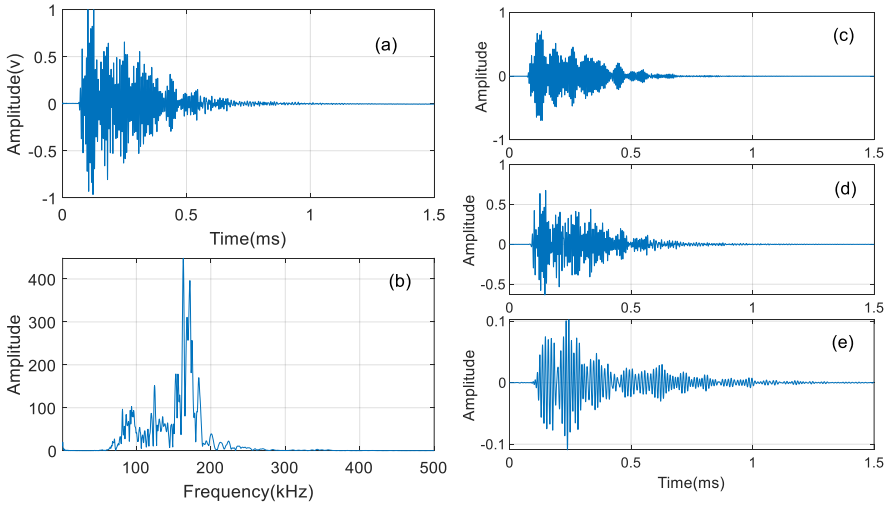

Figure 7. (a) Time domain signal, (b) frequency spectrum, (c) DWT coefficient cD_5 (156–312 kHz), (d) DWT coefficient cD_6 (78–156 kHz), and (e) DWT coefficient cD_7 (39–78 kHz).

4. MACHINE LEARNING MODELS

In this work, several models were used for the ASR expansion predictions, including linear regression, support vector regression, shallow neural network, and deep neural network approaches. The deep neural network uses the time domain signals as the feature input, whereas the other models use the extracted 13 features as the model input. Linear regression is a linear statistical approach to model the relationship between the response and one or more variables. It is represented by the equation below:

$$y = X\beta + \varepsilon, \tag{1}$$

where y is the response (i.e., the volumetric expansion of the concrete samples), X is the vector of the variables (i.e., the extracted features), β is the parameter vector, and ε is the error term. In this work, the parameter vector β is fitted using the data from the ASR sample, and the fitted linear regression model is tested using the ASR-2D sample. The linear regression model is optimized in MATLAB, and the final model contains an intercept term, linear and squared terms for each variable, and all products of pairs of distinct variables.

Support vector regression (SVR) is an ML algorithm used for regression tasks. It is based on the principles of support vector machines (SVMs), which are primarily used for classification tasks. SVM aims to find a hyperplane that best fits the training data while maximizing the margin (distance) between the hyperplane and the closest data points, known as *support vectors*. The key idea behind SVM is to map the input data into a higher-dimensional feature space, where a linear relationship can be more easily identified. SVM allows for nonlinear relationships by using kernel functions to implicitly map the data into this higher-dimensional space. The SVR model seeks to minimize the prediction error while controlling the deviations within a predefined margin called the epsilon tube. It strives to find a hyperplane that maintains a balance between fitting the training data and generalizing well to unseen data. The objective of the model is to minimize both the training error and the complexity of the solution, known as the regularization term. The SVM model was optimized in MATLAB using the ASR sample data. The optimized SVR model has a Gaussian kernel function with a kernel scale of 36.1, box constraint of 689.0, and epsilon tube width of 0.000146.

An artificial neural network is a connected graph with multiple layers, and each layer contains multiple nodes (neurons). A shallow feed-forward neural network has a relatively simple structure, with one input layer, one to two intermediate (hidden) layers, and one output layer. Lippmann [22] suggested that a multi-layer perceptron with two hidden layers is sufficient for creating classification regions of any desired shape. Another critical hyperparameter is the activation function, which defines the output of the node given the input or a set of inputs. Typical activation functions include the Gaussian, sigmoid, hyperbolic tangent, and radial basis functions (RBF). The parameters in the hidden layers can be optimized to achieve the best model performance. The optimized neural network used in this work has two hidden layers, in addition to the input and output layers. The first hidden layer contains 16 neurons, and the second hidden layer has 8 neurons with *relu* activation functions for both layers. A randomly selected 25% of the training data was used as the validation data.

Deep neural networks (DNNs) are a relatively recent addition to ML and are essentially artificial neural networks with more than two hidden layers. Inputs to the neural network can be time domain–related features, frequency domain–related features, or wavelet features. The time domain signal or frequency spectrum is also used as input for the ML models. Figure 8 shows the network structure of the DNN used herein; it has three hidden layers with *relu* activation functions. The input layer has 512 neurons, and the second hidden layer has 128 neurons. The third and fourth hidden layer have 32 and 8 neurons, respectively. To prevent the overfitting of the DNN, dropout layers are added to the network. The first and second dropout

layer both have a dropout rate of 0.4, whereas the last one has a rate of 0.3. Since the original time domain signal contains 10,000 samples, it is too large to be used as the input. To reduce the computational cost, the original time domain signal is cropped to 7,000 by deleting 3,000 samples in the unimportant, tail region of the signal. Next, the cropped signal is downsampled to 512 samples with a ratio of 13. The original sampling rate is 10 MHz. After downsampling, the new sampling rate is approximately 769 kHz, which is large enough to accommodate a signal with a main frequency band of 50 kHz to 250 kHz.

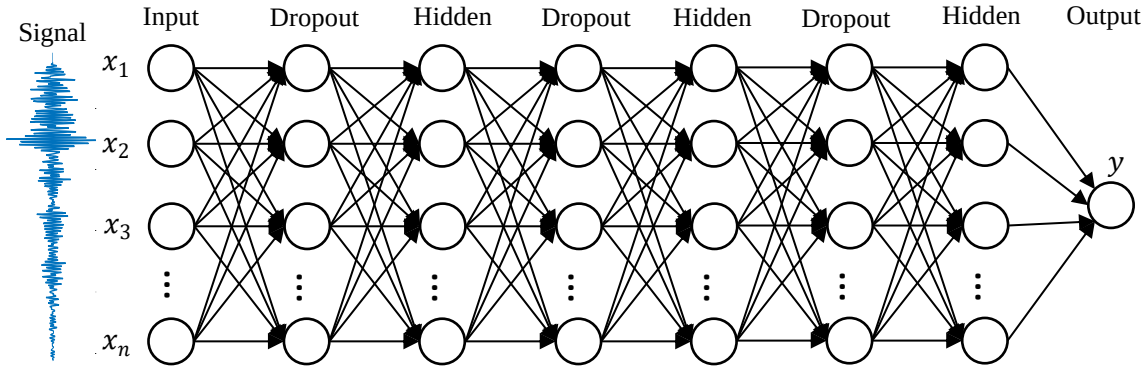

Figure 8. The network structure of the deep neural network model.

5. RESULTS

5.1 LR, SVR, AND SHALLOW NN WITHOUT FEATURE SELECTION

The ASR sample dataset is initially utilized as training data to establish models based on linear regression (LR), SVR, and shallow neural networks, incorporating all 13 variables. These developed models are subsequently put to the test with datasets derived from the ASR-2D sample. Figure 9 to Figure 11 illustrate the measured versus predicted expansion through different modeling techniques. In Figure 9, the LR model shows a good correlation, denoted by a high R^2 (i.e., $R^2 = 0.9982$) value, between the predicted and actual expansion in the ASR sample. Conversely, when applied to the ASR-2D data, the LR model performs sub-optimally, as indicated by a reduced R^2 (i.e., $R^2 = 0.7070$) and increased root mean square error (RMSE). Figure 10 delineates the correlation of measured and predicted expansion utilizing the SVR model on both ASR and ASR-2D samples. Whereas the training phase (Figure 10(a)) presents a relatively high R^2 of 0.9710 and a relatively small RMSE, the testing phase reveals a smaller R^2 and larger error than that seen in the LR model (i.e., $R^2 = 0.3245$ and RMSE = 0.1444%). This result suggests an overfitting situation for the SVR model, stemming from the application of the 13 input variables, thus leading to poor generalization when applied to the testing data. The shallow neural network's results, displayed in Figure 11, mimic those of the other two models: high R^2 and low RMSE in the training phase. However, it demonstrates disappointing performance in the testing phase, marked by a decreased R^2 and an increased RMSE. These outcomes suggest that even with a sophisticated neural network when employing unrelated features, the performance of the ML algorithm may still falter. Interestingly, despite its lower complexity, the LR model could potentially deliver superior results compared to the neural network.

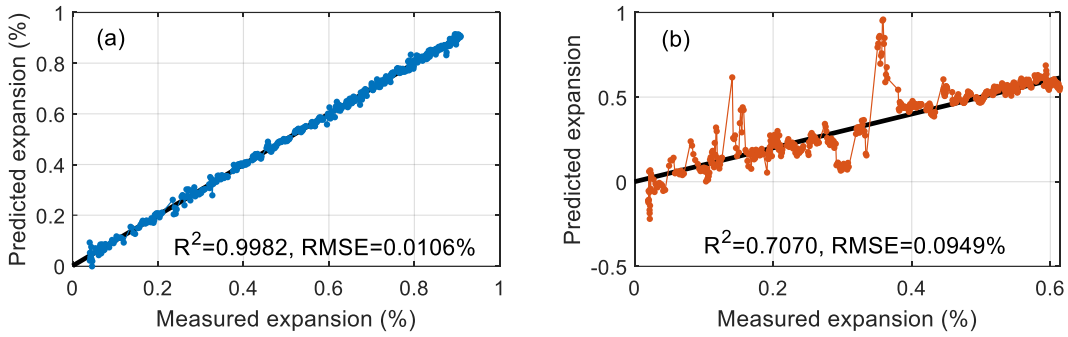

Figure 9. Measured expansion vs. predicted expansion using linear regression on the (a) ASR sample (training) and (b) ASR-2D sample (testing).

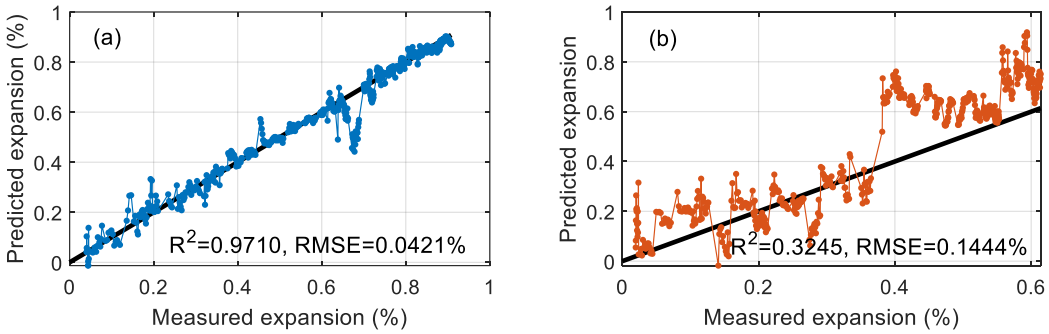

Figure 10. Measured expansion vs. predicted expansion using the SVR model on the (a) ASR sample, and (b) ASR-2D sample.

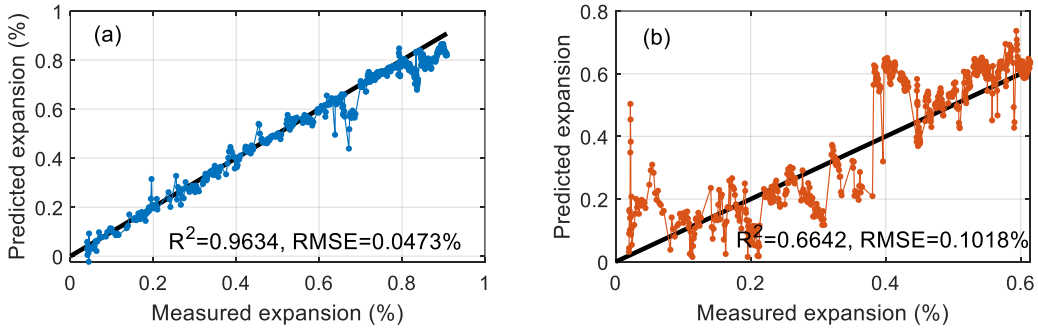

Figure 11. Measured expansion vs. predicted expansion using the shallow neural network model on the (a) ASR, and (b) ASR-2D samples.

5.2 LR, SVR, AND SHALLOW NN WITH FEATURE SELECTION

Because the SVR and shallow neural network models exhibit sufficient performance on the training data but show large prediction errors using the testing data, feature selection should be used to avoid overfitting and decrease the model variance. Correlation coefficients between the 13 features (wave velocity and detail coefficients) and the response (i.e., expansion) are summarized in Table 2 for the training (i.e., ASR) and testing (i.e., ASR-2D) datasets. The wave velocity has a high correlation with the volumetric expansion for both datasets. The features that have correlation coefficients larger than 0.5 for both datasets were selected.

Therefore, features 1, 3, 6, 7, 10, 11 were selected as input to the ML models, including the velocity, mean amplitude in the middle-frequency range (78 kHz – 156 kHz), maximum amplitude in the middle (78 kHz – 156 kHz) and low-frequency (39 kHz – 78 kHz) range, energy ratio in the frequency (39 kHz – 78 kHz) range, and attenuation in the high-frequency range (156 kHz – 312 kHz). Using these six features, the LR, SVR, and shallow neural network models performed better with adequate prediction accuracy. The training results and testing results with feature selection are shown in Figure 12 to Figure 14. In Figure 12, the training results exhibit a relatively higher R^2 and smaller RMSE compared to the results in Figure 9 using the same LR model. By using the features with relatively high correlations to the response, the testing results of the SVR model in Figure 13 were significantly improved, with an R^2 from 0.3245 to 0.8946 and an RMSE from 0.1444% to 0.0570%. The performance of the shallow neural network was also improved after using the selected features as the input. The R^2 and RMSE for all models without and with feature selection are summarized in Table 2. After feature selection, the R^2 for the training dataset has decreased for all three models, which might be an indication of elimination of overfitting. Compared with the prediction results without feature selections, all three models have improved prediction results on the ASR-2D sample with all selected six features. Thus, it can be concluded that the model selected may not significantly affect the prediction results; however, the features used will largely affect the model performance on the prediction.

Table 2. Absolute correlation coefficients between features and responses.

Feature	Vel.	Mean amplitude			Max amplitude			Energy			Attenuation		
		cD_5	cD_6	cD_7	cD_5	cD_6	cD_7	cD_5	cD_6	cD_7	cD_5	cD_6	cD_7
Index	**1**	2	**3**	4	5	**6**	**7**	8	9	**10**	**11**	12	13
ASR	0.92	0.52	0.87	0.67	0.83	0.76	0.86	0.66	0.41	0.84	0.81	0.43	0.05
ASR-2D	0.90	0.05	0.65	0.03	0.38	0.58	0.64	0.23	0.49	0.59	0.83	0.68	0.26

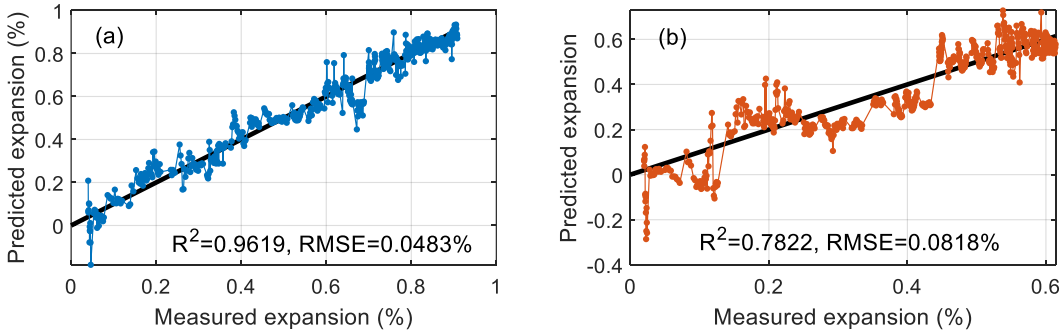

Figure 12. Measured expansion vs. predicted expansion using linear regression with feature selection on the (a) ASR sample (training) and (b) ASR-2D sample (testing).

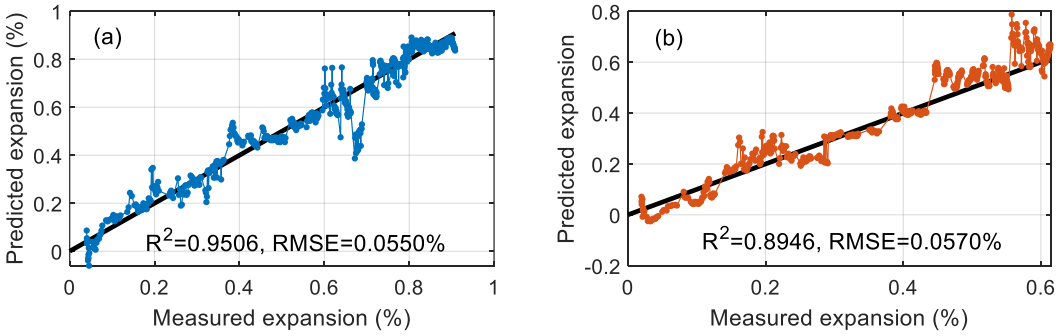

Figure 13. Measured expansion vs. predicted expansion using SVR with feature selection on the (a) ASR sample (training) and (b) ASR-2D sample (testing).

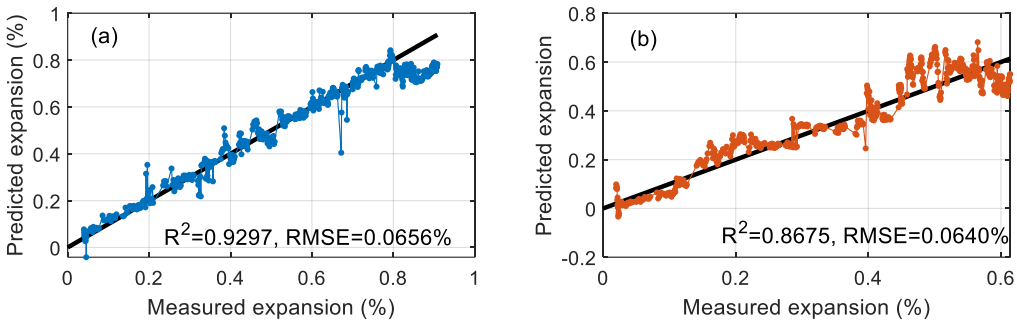

Figure 14. Measured expansion vs. predicted expansion using shallow neural network with feature selection on the (a) ASR sample and (b) ASR-2D sample.

Table 3. Prediction results of different learning models.

Method	ASR (training)		ASR-2D (testing)	
	R^2	RMSE	R^2	RMSE
LR	0.9982	0.0106%	0.7070	0.0949%
LR with feature selection	0.9619	0.0483%	0.7822	0.0818%
SVR	0.9710	0.0421%	0.3245	0.1444%
SVR with feature selection	0.9506	0.0550%	0.8946	0.0570%
Shallow NN	0.9634	0.0473%	0.6642	0.1018%
Shallow NN with feature selection	0.9297	0.0656%	0.8675	0.0640%

5.3 DEEP NEURAL NETWORK

The deep neural network model utilizes time domain signals as input features. In Figure 15, the learning curves (i.e., loss histories) of the deep neural network trained with the ASR sample data are depicted. After 100 epochs, both the training and validation loss reached a stable state with negligible values, suggesting a well-fitting DNN model. Figure 16 illustrates the training and testing results, presenting the measured expansion versus the predicted expansion. The training results exhibit a strong predictive capability, characterized by a high R^2 value and a low RMSE. Similarly, the testing results displayed a favorable R^2 value and a small RMSE. Notably, the test results obtained using the DNN model were comparable to the prediction results obtained with linear regression and feature selection, exhibiting similar R^2 and RMSE values. An important advantage of the DNN is its ability to achieve such performance without requiring feature engineering, encompassing feature extraction and feature selection. This finding underscores that the DNN can attain prediction performance on par with conventional regression models while obviating the need for laborious feature engineering processes. In this work, only the time domain signal was used as the input of the deep learning model. The frequency spectrum can also be used as the input of the deep learning model.

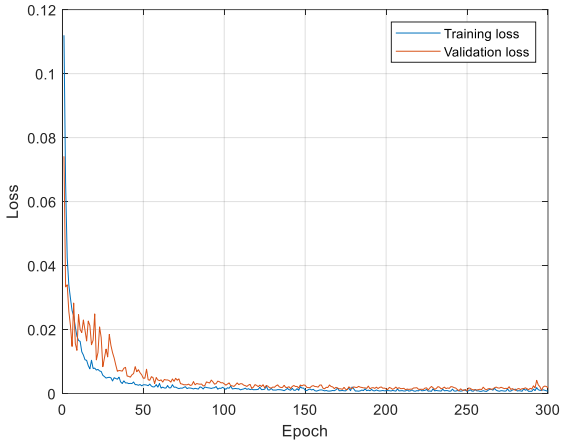

Figure 15. The learning curve of the DNN model trained with ASR sample data.

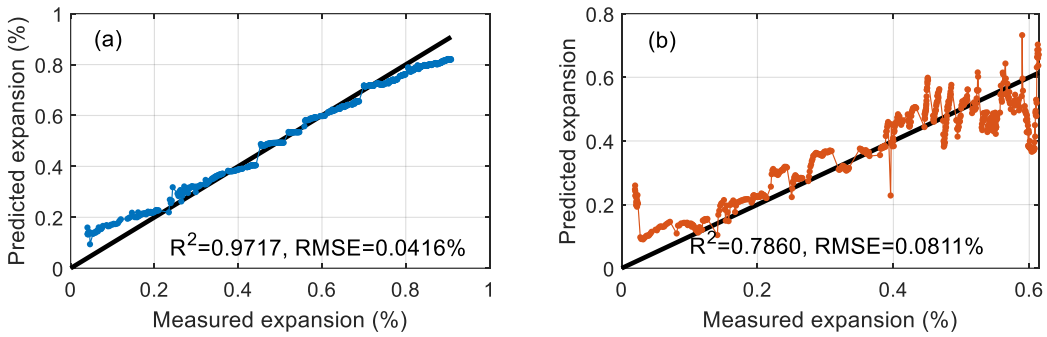

Figure 16. Measured expansion vs. predicted expansion using deep neural network on the (a) ASR sample and (b) ASR-2D sample.

6. CONCLUDING REMARKS

This study aimed to predict the volumetric expansion caused by ASR damage using ML models based on long-term ultrasonic monitoring signals. Ultrasonic signals and concrete expansion data were collected from two large concrete specimens with induced ASR. Four ML models were investigated in this work: LR, SVR, shallow neural network, and DNN approaches. For the first three models, a total of 13 features were extracted from the time domain signals of the ASR samples and used as input for training the ML models. The expansion prediction was tested on the ASR-2D sample. The extracted features included wave velocity and wavelet features calculated using wavelet transform of the time domain signals. In the case of the DNN model, the time domain signals themselves were used as input. Prior to inputting into the ML model, the signals were preprocessed through normalization and downsampling to reduce computational costs. All models were optimized using the training data from the ASR sample.

The results indicate that the prediction performance on the ASR-2D sample by the LR, SVR, and shallow neural network models were unsatisfactory, as evidenced by low R^2 values and large RMSE values (Table 3). The extracted wave velocity exhibits poor accuracy due to transducer reinstallation during the monitoring period and the presence of significant noise in some ultrasonic signals. The inclusion of all 13 features in the three regression models resulted in overfitting. However, after performing feature selection, six features were selected as the inputs, leading to improved performance of the three regression models with R^2 values above 0.78 and RMSE values below 0.082%. The performance of the three models did not

exhibit significant differences. Consequently, it can be concluded that the selection of features used in ML models has a greater impact on performance than the choice of a model when predicting expansion based on ultrasonic signals. The DNN employed time domain signals directly as input, eliminating the need for feature extraction and selection. Notably, the model's performance was found to be comparable to that of other regression models, such as LR, SVR, and shallow neural networks. This observation highlights the potential of the deep learning model as a reliable prediction tool for assessing concrete sample damage through ultrasonic NDE signal processing.

It is important to note that the prediction procedure described in this study was justified for the ASR and ASR-2D samples, which shared the same mix design and underwent similar ASR development processes. However, it should also be acknowledged that this prediction procedure may not be reliably applicable if the two mix designs differ significantly. Future work will include the investigation of factors that affect the performance of the ML model for concrete damage assessment based on ultrasonic NDE data.

7. REFERENCE

[1] M. Kawamura and K. Iwahori, "ASR gel composition and expansive pressure in mortars under restraint," *Cement and Concrete Composites*, vol. 26, no. 1, pp. 47–56, Jan. 2004.

[2] B. Fournier, M.-A. Berube, K. J. Folliard, and M. Thomas, "Report on the Diagnosis, Prognosis, and Mitigation of Alkali-Silica Reaction (ASR) in Transportation Structures," Art. no. FHWA-HIF-09-001, Jan. 2010.

[3] F. Saint-Pierre, P. Rivard, and G. Ballivy, "Measurement of alkali–silica reaction progression by ultrasonic waves attenuation," *Cement and Concrete Research*, vol. 37, no. 6, pp. 948–956, Jun. 2007.

[4] E. R. Giannini, "Evaluation of concrete structures affected by alkali-silica reaction and delayed ettringite formation," thesis, 2012.

[5] T. Ju, J. D. Achenbach, L. J. Jacobs, M. Guimaraes, and J. Qu, "Ultrasonic nondestructive evaluation of alkali–silica reaction damage in concrete prism samples," *Mater Struct*, vol. 50, no. 1, p. 60, Aug. 2016.

[6] H. Sun, Y. Tang, C. Malone, and J. Zhu, "Long-term ultrasonic monitoring of concrete affected by alkali-silica reaction," *Structural Health Monitoring*, p. 14759217231169000, Apr. 2023, doi: 10.1177/14759217231169000.

[7] K. Amini, M. Jalalpour, and N. Delatte, "Advancing concrete strength prediction using non-destructive testing: Development and verification of a generalizable model," *Construction and Building Materials*, vol. 102, pp. 762–768, Jan. 2016.

[8] M. A. Kewalramani and R. Gupta, "Concrete compressive strength prediction using ultrasonic pulse velocity through artificial neural networks," *Automation in Construction*, vol. 15, no. 3, pp. 374–379, May 2006.

[9] D. Feng *et al.*, "Machine learning-based compressive strength prediction for concrete: An adaptive boosting approach," *Construction and Building Materials*, vol. 230, p. 117000, Jan. 2020.

[10] G. Trtnik, F. Kavčič, and G. Turk, "Prediction of concrete strength using ultrasonic pulse velocity and artificial neural networks," *Ultrasonics*, vol. 49, no. 1, pp. 53–60, Jan. 2009.

[11] S. Sambath, P. Nagaraj, and N. Selvakumar, "Automatic Defect Classification in Ultrasonic NDT Using Artificial Intelligence," *J Nondestruct Eval*, vol. 30, no. 1, pp. 20–28, Mar. 2011.

[12] L. C. Silva, E. F. Simas Filho, M. C. S. Albuquerque, I. C. Silva, and C. T. T. Farias, "Segmented analysis of time-of-flight diffraction ultrasound for flaw detection in welded steel plates using extreme learning machines," *Ultrasonics*, vol. 102, p. 106057, Mar. 2020, doi: https://doi.org/10.1016/j.ultras.2019.106057.

[13] Ó. Martín, M. López, and F. Martín, "Artificial neural networks for quality control by ultrasonic testing in resistance spot welding," *Journal of Materials Processing Technology*, vol. 183, no. 2, pp. 226–233, Mar. 2007.

[14] H. Sun, J. Zhu, and P. Ramuhalli, "Machine Learning of Ultrasonic Data for Expansion Prediction of Concrete with Alkali-Silica Reaction," in *STRUCTURAL HEALTH MONITORING 2021*, 2021. doi: 10.12783/shm2021/36321.

[15] D. A. Clayton, H. Santos-Villalobos, N. D. B. Ezell, J. Clayton, and J. Baba, "Automated Detection of Alkali-Silica Reaction in Concrete Using Linear Array Ultrasound Data," in *Proceedings of the 18th International Conference on Environmental Degradation of Materials in Nuclear Power Systems – Water Reactors*, J. H. Jackson, D. Paraventi, and M. Wright, Eds., in The Minerals, Metals & Materials Series. Cham: Springer International Publishing, 2019, pp. 1335–1345. doi: 10.1007/978-3-030-04639-2_87.

[16] T. Shin, H. Sun, J. Zhu, and Y. Zhang, "Nondestructive Damage Detection of Concrete With Alkali-Silica Reactions Using Coda Wave and Anomaly Detection," *IEEE Sensors Journal*, vol. 22, no. 6, pp. 6124–6135, Mar. 2022, doi: 10.1109/JSEN.2022.3149721.

[17] C. Malone, “Quantitative Assessment of Alkali-Silica Reaction in Small and Large-Scale Concrete Specimens Utilizing Nonlinear Acoustic Techniques,” *Civil and Environmental Engineering Theses, Dissertations, and Student Research*, Aug. 2020.
[18] J. Zhu *et al.*, “Online Monitoring System for Concrete Structures Affected by Alkali-Silica Reaction,” Univ. of Nebraska, Lincoln, NE (United States), DOE-UNL-NE8544, Dec. 2021. doi: 10.2172/1838356.
[19] H. Sun, “Thermal Modulation of Nonlinear Ultrasonic Waves,” Ph.D., The University of Nebraska - Lincoln, United States -- Nebraska. Accessed: Jun. 01, 2023. [Online]. Available: https://www.proquest.com/docview/2444913300/abstract/D84F623EF6674299PQ/1
[20] N. Maeda, “A Method for Reading and Checking Phase Time in Auto-Processing System of Seismic Wave Data,” *Zisin (Journal of the Seismological Society of Japan. 2nd ser.)*, vol. 38, no. 3, pp. 365–379, 1985.
[21] R. Polikar, L. Udpa, S. Udpa, and V. Honavar, “An incremental learning algorithm with confidence estimation for automated identification of NDE signals,” *IEEE Transactions on Ultrasonics, Ferroelectrics, and Frequency Control*, vol. 51, no. 8, pp. 990–1001, Aug. 2004.
[22] R. Lippmann, “An introduction to computing with neural nets,” *IEEE ASSP Magazine*, vol. 4, no. 2, pp. 4–22, Apr. 1987, doi: 10.1109/MASSP.1987.1165576.